



Publication Year	2018
Acceptance in OA @INAF	2020-11-09T16:18:16Z
Title	Large Binocular Telescope observations of PSR J2043+2740*
Authors	TESTA, Vincenzo; MIGNANI, Roberto; Rea, N.; MARELLI, MARTINO; Salvetti, D.; et al.
DOI	10.1093/mnras/stx2512
Handle	http://hdl.handle.net/20.500.12386/28240
Journal	MONTHLY NOTICES OF THE ROYAL ASTRONOMICAL SOCIETY
Number	473

Large Binocular Telescope observations of PSR J2043+2740^{*}

V. Testa^{1†}, R. P. Mignani^{2,3}, N. Rea^{4,5}, M. Marelli², D. Salvetti², A. A. Breeveld⁶, F. Cusano⁷, R. Carini¹

¹ INAF - Osservatorio Astronomico di Roma, via Frascati 33, 00078, Monte Porzio Catone, Rome, Italy

² INAF - Istituto di Astrofisica Spaziale e Fisica Cosmica Milano, via E. Bassini 15, 20133, Milano, Italy

³ Janusz Gil Institute of Astronomy, University of Zielona Góra, Lubuska 2, 65-265, Zielona Góra, Poland

⁴ Institute of Space Sciences (IEECCSIC), Carrer de Can Magrans s/n, E-08193 Barcelona, Spain

⁵ Anton Pannekoek Institute for Astronomy, University of Amsterdam, Postbus 94249, NL-1090-GE Amsterdam, The Netherlands

⁶ Mullard Space Science Laboratory, University College London, Holmbury St. Mary, Dorking, Surrey, RH5 6NT, UK

⁷ INAF - Osservatorio Astronomico di Bologna, via Gobetti 93/3, 40129 Bologna, Italy

Accepted 2017 September 24. Received 2017 September 8; in original form 2017 June 30

ABSTRACT

We present the results of deep optical imaging of the radio/ γ -ray pulsar PSR J2043+2740, obtained with the Large Binocular Telescope (LBT). With a characteristic age of 1.2 Myr, PSR J2043+2740 is one of the oldest (non recycled) pulsars detected in γ -rays, although with still a quite high rotational energy reservoir ($\dot{E}_{\text{rot}} = 5.6 \times 10^{34} \text{ erg s}^{-1}$). The presumably close distance (a few hundred pc), suggested by the hydrogen column density ($N_{\text{H}} \lesssim 3.6 \times 10^{20} \text{ cm}^{-2}$), would make it a viable target for deep optical observations, never attempted until now. We observed the pulsar with the Large Binocular Camera of the LBT. The only object ($V=25.44 \pm 0.05$) detected within $\sim 3''$ from the pulsar radio coordinates is unrelated to it. PSR J2043+2740 is, thus, undetected down to $V \sim 26.6$ (3σ), the deepest limit on its optical emission. We discuss the implications of this result on the pulsar emission properties.

Key words: stars: neutron – pulsars: individual:

1 INTRODUCTION

The launch of the *Fermi* Gamma-ray Space Telescope has spurred on the search for pulsars in γ -rays (Grenier & Harding 2015), yielding over 200¹ detections and triggering multi-wavelength observations. While pulsars are common targets in the X-rays, they are very challenging targets in the optical and very few of them have been identified (see Mignani et al. 2016 and references therein). Here we report on Large Binocular Telescope (LBT) observations of an isolated pulsar, PSR J2043+2740, detected by both *AGILE* (Pellizzoni et al. 2009) and *Fermi* (Abdo et al. 2010; Noutsos et al. 2011). It was discovered as a radio pulsar (Ray et al. 1996) and later on as an X-ray source by *XMM-Newton* (Becker et al. 2004), although X-ray pulsations have not yet been found. PSR J2043+2740 is one of the very few non-recycled pulsars older than

1 Myr detected in γ -rays, with a characteristic age $\tau_c = 1.2$ Myr, inferred from the values of its spin period $P_s = 0.096$ s and its derivative $\dot{P}_s = 1.27 \times 10^{-15} \text{ s s}^{-1}$ (Ray et al. 1996). This also yields a rotational energy loss rate $\dot{E}_{\text{rot}} = 5.6 \times 10^{34} \text{ erg s}^{-1}$ and a surface dipolar magnetic field $B_s = 3.54 \times 10^{11} \text{ G}^2$. Although PSR J2043+2740 does not have a very large spin-down power compared to young (~ 1 – 10 kyr) pulsars ($\sim 10^{36}$ – $10^{38} \text{ erg s}^{-1}$), it is still a factor of two larger than that of middle aged γ -ray pulsars (~ 0.1 – 0.5 Myr), such as Geminga, PSR B0656+14, and PSR B1055–52, all detected in the optical thanks to their distances $\lesssim 500$ pc (Abdo et al. 2013). The distance to PSR J2043+2740 is uncertain owing to the lack of a radio parallax measurement. The radio dispersion measure ($\text{DM} = 21.0 \pm 0.1 \text{ pc cm}^{-3}$; Ray et al. 1996) gives a distance of 1.8 ± 0.3 kpc from the NE2001 model of the Galactic free electron density (Cordes & Lazio 2002). A slightly smaller distance (1.48 kpc) is inferred from the model of Yao et al. (2017). The hydrogen column density towards the pulsar obtained from the X-ray spectral fits ($N_{\text{H}} \lesssim 3.6 \times 10^{20} \text{ cm}^{-2}$; Abdo et al. 2013) suggests a distance of a few hundred pc (He et al. 2013), although these estimates depend on the model X-ray spectrum. Such a distance would make PSR J2043+2740 a viable target for deep optical observations, never carried out until now, and might be compatible

^{*} The LBT is an international collaboration among institutions in the United States, Italy and Germany. LBT Corporation partners are: The University of Arizona on behalf of the Arizona university system; Istituto Nazionale di Astrofisica, Italy; LBT Beteiligungsgesellschaft, Germany, representing the Max-Planck Society, the Astrophysical Institute Potsdam, and Heidelberg University; The Ohio State University, and The Research Corporation, on behalf of The University of Notre Dame, University of Minnesota and University of Virginia.

[†] E-mail: vincenzo.testa@oa-roma.inaf.it

¹ <https://confluence.slac.stanford.edu/display/GLAMCOG/>

² Derived from the magnetic dipole model, e.g. Kaspi & Kramer (2016).

with the debated association (Noutsos et al. 2011) with the Cygnus Loop supernova remnant (SNR) at 540_{-80}^{+100} pc (Blair et al. 2005).

The structure of this manuscript is as follows: observations and data reduction are described in Sectn. 2, whereas the results are presented and discussed in Sectn. 3 and 4, respectively.

2 OBSERVATIONS AND DATA ANALYSIS

The PSR J2043+2740 observations were carried out on July 5th, 2016 with the LBT at the Mount Graham International Observatory (Arizona, USA) and the Large Binocular Camera (LBC; Gilalongo et al. 2008). The Camera's field of view is $23' \times 25'$, with a pixel scale of $0''.2255$. The images were taken through the filters SDT-USpec, V-BESSEL, and i-SLOAN, closely matching the Sloan filters u and i (Fukugita et al. 1996), and the Johnson V filter. For each filter, three sets of exposures were acquired with exposure times of 20s, 60s and 120s, for a total integration of 5887 s (Uspec and i-SLOAN) and 5376 s (V-BESSEL). Sky conditions were non-photometric owing to the presence of cirri and the average seeing was around $1''.2$. The target was observed with an average airmass around 1.01 and 1.09, and with a lunar illumination of $\sim 1\%$. Images were reduced with the LBC data reduction pipeline, correcting raw science frames for bias, dark and flat fields. A further low-order flat-field correction was obtained from the night sky flats to remove large-scale effects. We, then, corrected the images for geometrical distortions, applying a linear pixel scale resampling. Finally, we stacked all images taken with the same filter and used the master frames to compute the astrometric solution ($\sim 0''.1$ rms).

Since the night was non-photometric, we performed the photometric calibration directly on the science frames by matching stars in public source catalogues. In particular, for the SDT-USpec filter we used a source list extracted from the *XMM-Newton* Serendipitous Ultra-violet Source Survey Catalogue version 3.0 (XMM-SUSS3³), built from observations with the *XMM-Newton* Optical Monitor (OM; Mason et al. 2001), whereas for both the V-BESSEL and i-SLOAN filters we used a source list from the American Association of Variable Stars Observers (AAVSO) Photometric All-Sky Survey⁴ (APASS). All magnitudes are in the AB system (Oke 1974). For all filters, we computed object photometry with the DAOPHOT II software package (Stetson 1994) following a standard procedure for source detection, modelling of the image point spread function (PSF), and multi-band source catalogue generation (see, e.g., Testa et al. 2015). After accounting for photometric errors, the fit residuals turned out to be ~ 0.01 magnitudes in all filters, to which we must add the average absolute photometry accuracy of SUSS3 and APASS, which is ~ 0.05 magnitudes.

3 RESULTS

Fig. 1 shows a zoom of the i-band image centred around the pulsar position. The J2000 coordinates of PSR J2043+2740 used by Noutsos et al. (2011) are: $\alpha = 20^{\text{h}}43^{\text{m}}43^{\text{s}}.52$; $\delta = +27^{\circ}40'56''.06$ but with no quoted error. The ATNF pulsar catalogue (Manchester et al. 2005) reports the same coordinates, with an uncertainty of $0''.1$ and $1''$ in right ascension and declination, respectively, at a reference epoch MJD=49773. Owing to timing noise, no updated pulsar coordinates could be computed using the timing model of Kerr et

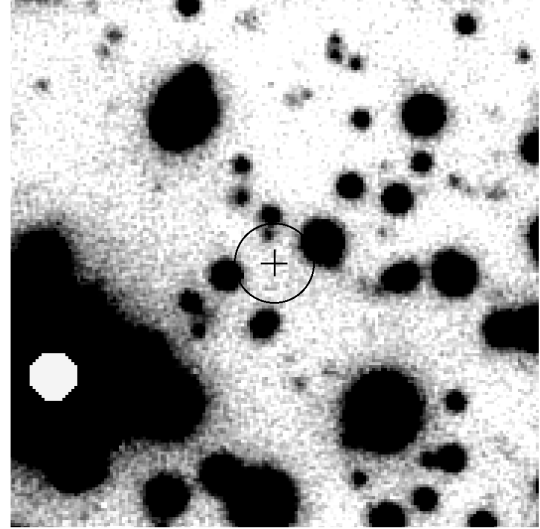


Figure 1. Zoom of the PSR J2043+2740 field ($20'' \times 20''$) obtained in the i band (5887 s) and centred on the pulsar position (cross). North to the top, east to the left. The length of the cross arms ($1''$) is equal to the nominal uncertainty on the radio coordinates. The circle ($3''$ radius) indicates the search region assumed to account for the unknown pulsar proper motion.

al. (2015). PSR J2043+2740 has not been observed by *Chandra*, so that we cannot rely on an accurate, model-independent position. No proper motion has been measured for PSR J2043+2740. Therefore, to account for its unknown angular displacement between the epoch of the reference radio position and that of our LBT observations (MJD=57574), we looked for candidate counterparts within a conservative search region of $3''$ radius. This is three times as large as the formal radio position uncertainty and roughly equal to the angular displacement expected for a pulsar moving with an average transverse velocity of 400 km s^{-1} (Hobbs et al. 2005) at a distance as close as the Cygnus Loop SNR (540_{-80}^{+100} pc; Blair et al. 2005).

Only one object is detected within the search region ($3''$ radius) defined above (Fig. 1). The object is barely visible in the V band and not in the U band, whereas it is clearly detected in the i band. Its magnitudes have been computed following the same procedure as described in Sectn. 2 and are $V=25.44 \pm 0.05$, $i=25.08 \pm 0.08$, $U > 26.5$ (AB). To investigate the characteristics of the object, we built a U–V vs V–i colour-colour diagram (CCD) of all objects within $5'$ from the pulsar position and compared its colours with respect to the main sequence (Fig. 2). Since the field stars are, presumably, at different distances with respect to the pulsar, the diagram is uncorrected for the reddening. The object's colours are $V-i = 0.36 \pm 0.09$, $U-V > 1.06$ and are close to those of the main sequence. This means that it does not stand out for having peculiar colours, as one would expect for a pulsar, which is usually characterised by blue colours (e.g., Mignani & Caraveo 2001; Mignani et al. 2010). We compared the observed CCD to a synthetic one computed with the Besançon Model of Stellar Population Synthesis to simulate the Galactic stellar population within a $5'$ radius around the direction of PSR J2043+2740. As shown in Fig. 2, the main sequence of the observed CCD is consistent with the model Galactic stellar population, supporting the conclusion that the object is a field star rather than the pulsar. Estimated 3σ -level limiting magnitudes are 26.5, 26.6, and 26.2 in the U, V and i bands, respectively, which we assume as upper limits on the pulsar fluxes.

³ <https://www.cosmos.esa.int/web/xmm-newton/xsa>

⁴ <http://www.aavso.org/apass>

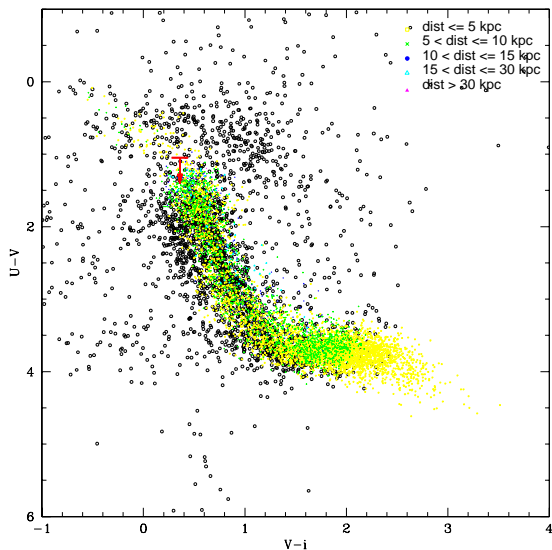


Figure 2. Synthetic CCD for the Galactic stellar population (in colour for different distances) in the pulsar direction simulated with the Besançon model (Robin et al. 2004), superimposed to the observed one (black). The spread in the synthetic CCD is the effect of the distance-dependent reddening correction, applied by the model, and the simulated photometric error.

Table 1. Comparison between the optical properties of PSR J2043+2740 and the two pulsars closest in age detected in the optical.

	B1055–52	J2043+2740	B1929+10
τ_c (Myr)	0.5	1.2	3
\dot{E}_{rot} (10^{34} erg s $^{-1}$)	3.0	5.6	0.39
L_{opt} (10^{27} erg s $^{-1}$)	3.74	$\lesssim 22.0$	1.04
η_{opt} (10^{-7})	1.26	$\lesssim 3.93$	2.7
$F_{\text{opt}}/F_{\gamma}$ (10^{-6})	0.88	$\lesssim 7.14$	$\gtrsim 31.1$
$F_{\text{opt}}/F_{\text{X}}$ (10^{-4})	16.9	$\lesssim 5.57$	3.4

4 DISCUSSION

Our observations of PSR J2043+2740 are much deeper than those obtained by Beronya et al. (2015) with the BTA (Bolshoi Teleskop Alt-azimutalnyi) 6m telescope, which only yielded a 3σ limit of $R \sim 21.7$ (Vega) on the pulsar flux. The pulsar is obviously too faint to have been detected in the *XMM-Newton* OM images (Becker et al. 2004), with 3σ limits of $B \approx 21.5$ and $U \approx 20.9$ (Vega).

We checked whether our limits on the pulsar flux could help to prove or disprove the association with the Cygnus Loop SNR. In general, the non-thermal optical luminosity L_{opt} of rotation-powered pulsars scales with a power of the rotational energy loss rate (see, e.g. Mignani et al. 2012) as $L_{\text{opt}} \propto \dot{E}_{\text{rot}}^{1.70 \pm 0.03}$ (1σ statistical error). From this relation, we estimate a luminosity of $\sim 3.16 \times 10^{27}$ erg s $^{-1}$ for PSR J2043+2740, corresponding to a magnitude $V \sim 26.2$ – 26.9 at the distance of the Cygnus Loop SNR, after accounting for the interstellar reddening $E(B - V) \lesssim 0.06$, inferred from the N_{H} (Predehl & Schmitt 1995). Therefore, our detection limit ($V \sim 26.6$) does not determine whether the pulsar is at the distance of the Cygnus Loop SNR, and their association remains uncertain. Pushing the limit on the pulsar brightness down to $V \sim 28$ would imply a distance larger than ~ 1 kpc for the same predicted optical luminosity and would disprove this association.

Given the lack of a counter-evidence, we assume the pulsar DM-based distance (Yao et al. 2017) as a reference.

We compared our constraints on the optical emission of PSR J2043+2740 with the properties of other pulsars of comparable age identified in the optical (Table 1). Among them, PSR J2043+2740 lies somewhere in between the middle-aged pulsars, with the oldest being PSR B1055–52 ($\tau_c \sim 0.5$ Myr), and the oldish ones, such as PSR B1929+10 ($\tau_c \sim 3$ Myr). The V-band optical luminosity of PSR J2043+2740 is $L_{\text{opt}} \lesssim 2.2 \times 10^{28} d_{1.48}^2$ erg s $^{-1}$, where $d_{1.48}$ is its distance in units of 1.48 kpc (Yao et al. 2017). If one assumes that the V-band optical emission is entirely non-thermal and rotation powered, its emission efficiency would be $\eta_{\text{opt}} \lesssim 3.93 \times 10^{-7} d_{1.48}^2$. For comparison, for a distance of 0.35 kpc (Mignani et al. 2010), the V-band optical luminosity of PSR B1055–52 would be 3.74×10^{27} erg s $^{-1}$ and its emission efficiency 1.26×10^{-7} . We note that the optical spectrum of PSR B1055–52 brings the contribution of both non-thermal emission from the magnetosphere and thermal emission from the neutron star surface and is the combination of a power-law (PL) and a Rayleigh-Jeans (R-J) (Mignani et al. 2010), as observed in other middle-aged pulsars. However, the contribution of the R-J in the V band is about an order of magnitude smaller than that of the PL, so that its V-band luminosity is essentially non thermal. The γ -ray energy flux above 100 MeV for PSR J2043+2740 is $F_{\gamma} = (1.18 \pm 0.12) \times 10^{-11}$ erg cm $^{-2}$ s $^{-1}$

(Acerro et al. 2015), whereas its unabsorbed non-thermal X-ray flux (0.3–10 keV) is $F_{\text{X}} = 0.22_{-0.11}^{+0.03} \times 10^{-13}$ erg cm $^{-2}$ s $^{-1}$ (Abdo et al. 2013), which gives an optical-to- γ -ray flux ratio $F_{\text{opt}}/F_{\gamma} \lesssim 7.14 \times 10^{-6}$ and an optical-to-X-ray flux ratio $F_{\text{opt}}/F_{\text{X}} \lesssim 5.57 \times 10^{-4}$, where the optical flux F_{opt} has been corrected for the extinction. For PSR B1055–52, $F_{\gamma} = (2.90 \pm 0.03) \times 10^{-10}$ erg cm $^{-2}$ s $^{-1}$ and $F_{\text{X}} = 1.51_{-0.13}^{+0.02} \times 10^{-13}$ erg cm $^{-2}$ s $^{-1}$ (0.3–10 keV), yielding $F_{\text{opt}}/F_{\gamma} \sim 0.88 \times 10^{-6}$ and $F_{\text{opt}}/F_{\text{X}} \sim 16.9 \times 10^{-4}$, whereas for PSR B1929+10 the V-band optical luminosity would be 1.04×10^{27} erg s $^{-1}$ for a 0.31 kpc distance (Verbiest et al. 2012) and its emission efficiency $\sim 2.7 \times 10^{-7}$. However, PSR B1929+10 has not been observed in the optical but in the near-UV (Mignani et al. 2002) where the spectrum is modelled by a PL with spectral index $\alpha \sim 0.5$. Therefore, its extrapolation to the optical gives uncertain predictions on the unabsorbed V-band flux, and it is not possible to determine whether it decouples into a PL plus a R-J, like in PSR B1055–52 (Mignani et al. 2010). In this case, both the non-thermal optical luminosity and emission efficiency would be overestimated. PSR B1929+10 has been detected in the X-rays with an unabsorbed non-thermal 0.3–10 keV flux $F_{\text{X}} = 2.64_{-0.16}^{+0.12} \times 10^{-13}$ erg cm $^{-2}$ s $^{-1}$ (Becker et al. 2006), but not in γ -rays down to 2.9×10^{-12} erg cm $^{-2}$ s $^{-1}$ (Romani et al. 2011), yielding $F_{\text{opt}}/F_{\text{X}} \sim 3.4 \times 10^{-4}$ and $F_{\text{opt}}/F_{\gamma} \gtrsim 3.11 \times 10^{-5}$.

The γ -ray spectrum of PSR J2043+2740 is described by a PL with an exponential cut off, where photon index $\Gamma_{\gamma} = 1.44 \pm 0.25$ and cut off energy $E_c = 1.34 \pm 0.37$ GeV (Acerro et al. 2015). The *XMM-Newton* spectrum can be fit by a PL with $\Gamma_{\text{X}} = 2.98_{-0.29}^{+0.44}$ (Abdo et al. 2013). The addition of a blackbody component is compatible with the counting statistics, but an f -test (Bevington 1969) shows no improvement in the fit significance. We compared our optical flux measurements with the extrapolations of the high-energy spectra, after correcting for the reddening using the extinction coefficients of Fitzpatrick (1999). The spectral energy distribution (SED) of PSR J2043+2740 is shown in Fig. 3. As seen in other cases, the extrapolations of the two PL spectra are not compatible with each other, implying a turnover in the γ -ray PL at low energies. This is also observed in, e.g. the middle-aged pulsar PSR

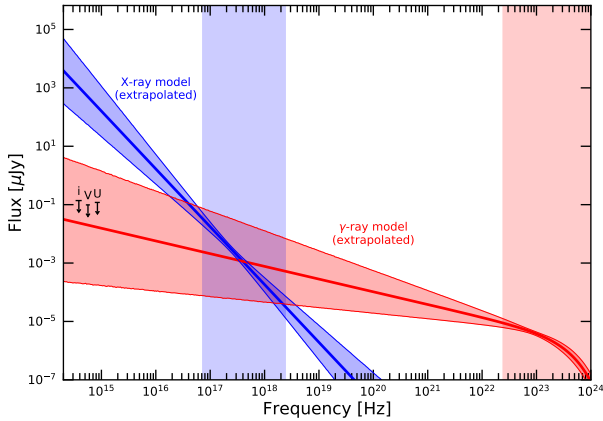


Figure 3. SED of PSR J2043+2740. The extinction-corrected optical flux upper limits are labelled with the band names. The blue and red lines are the extrapolation of the X and γ -ray PL spectra, respectively (Abdo et al. 2013; Acero et al. 2015), with their 1σ errors (dashed lines). The blue and red regions mark the range where the X and γ -ray spectra were measured.

B1055–52 (Mignani et al. 2010), although there is no apparent correlation between the presence of a turnover and the pulsar characteristic age. The optical flux upper limits are below the extrapolation of the assumed X-ray PL spectrum but are not deep enough to rule out that the optical emission might be compatible with the γ -ray PL extrapolation. This could be a rare case where the γ -ray and optical spectra are related to each other.

ACKNOWLEDGMENTS

We thank the anonymous referee for his/her considerate review. While writing this manuscript, we commemorated the fifth anniversary of the death of renown Italian astrophysicist Franco Pacini, who passed away on January 26th 2012. Franco authored many seminal publications on neutron stars since right before their discovery and was an active promoter of the LBT project. We dedicate our manuscript to his memory. RPM acknowledges financial support from an Occhialini Fellowship. This research was made possible through the use of the AAVSO Photometric All-Sky Survey (APASS), funded by the Robert Martin Ayers Sciences Fund.

REFERENCES

- Abdo A.A., et al., 2010, *ApJ*, 713, 154
 Abdo A.A., et al., 2013, *ApJS*, 298, 17
 Acero F., et al., 2015, *ApJS*, 218, 23
 Becker W., Weisskopf M. C., Tennant A. F., Jessner A., Dyks J., Harding A. K., Zhang S. N., 2004, *ApJ*, 615, 908
 Becker W. et al. 2006, *ApJ*, 645, 1421
 Beronya D. M., Shibano Yu A., Zyuzin D. A., Komarova V. N., 2015, 17th Russian Youth Conference on Physics and Astronomy, Journal of Physics: Conference Series 661
 Bevington P. R., 1969, *Data reduction and error analysis for the physical sciences*, McGraw-Hill
 Blair W. P., Sankrit R., Raymond J. C., 2005, *AJ*, 129, 2268
 Cordes J. M., & Lazio T. J. W., 2002, arXiv:astro-ph/0207156
 Fitzpatrick E. L., 1999, *PASP*, 111, 63

- Fukugita M., Ichikawa T., Gunn J. E., Doi M., Shimasaku K., Schneider D. P., 1996, *AJ*, 111, 1748
 Giallongo E., et al., 2008, *A&A*, 482, 349
 Grenier I. A. & Harding A. K., 2015, *Comptes rendus - Physique*, Vol. 16, Issue 6-7, p. 641
 He C., Ng C.-Y., Kaspi V. M., 2013, *ApJ*, 768, 64
 Hobbs G., Lorimer D. R., Lyne A. G., Kramer M., 2005, *MNRAS*, 360, 974
 Kaspi V. M. & Kramer M., 2016, *Proc. of the 26th Solvay Conference on Physics on Astrophysics and Cosmology*, R. Blandford & A. Sevrin eds., arXiv:1602.07738
 Kerr M., Ray P. S., Shannon R. M., Camilo F., 2015, *ApJ*, 814, 128
 Manchester R. N., Hobbs G. B., Teoh A. & Hobbs M., 2005, *AJ*, 129, 1993
 Mason K. O., et al., 2001, *A&A*, 365, 36
 Mignani R. P. & Caraveo P. A., 2001, *A&A*, 376, 213
 Mignani R. P., De Luca A., Caraveo P.A., Becker W., 2002, *ApJ*, 580, L47
 Mignani R. P., Pavlov G.G., Kargaltsev O., 2010, *ApJ*, 720, 1635
 Mignani R. P., De Luca A., Hummel W., Zajczyk A., Rudak B., Kanbach G., Słowikowska A., 2012, *A&A*, 544, 100
 Mignani R. P., et al., 2016, *MNRAS*, 461, 4317
 Oke J.B., 1974, *ApJS*, 27, 21
 Pellizzoni A., et al. 2009, *ApJ*, 695, L115
 Predehl P. & Schmitt J.H.M.M., 1995, *A&A*, 293, 889
 Ray P. S., et al., 1996, *ApJ*, 470, 1103
 Robin A.C., Reylé C., Derrière S., Picaud S., 2004, *A&A* 416, 157
 Romani R. W., Kerr M., Craig H. A., Johnston S., Cognard I., Smith D. A., 2011, *ApJ*, 738, 114
 Stetson P.B., 1994, *PASP*, 106, 250
 Testa V., Mignani R. P., Pallanca C., Corongiu A., Ferraro F. R., 2015, *MNRAS*, 453, 4159
 Verbiest J.P.W., et al., 2012, *ApJ*, 755, 39
 Yao J. N., Manchester R. N., Wang N., 2017, *ApJ*, 835, 29